IEEE Access
Multidisciplinary | Rapid Review | Open Access Journal

Received August 7, 2019, accepted August 28, 2019, date of publication September 11, 2019,
date of current version September 25, 2019.

Digital Object Identifier 10.1109/ACCESS.2019.2940921

Bradycardia and Tachycardia Detection Using a Synthesis-by-Analysis Modeling Approach of Pulsatile Signal

YONGXIN CHOU[1,4], JASON GU[2,5], JICHENG LIU[1], YA GU[1], AND JIAJUN LIN[3,4]
[1]School of Electrical and Automatic Engineering, Changshu Institute of Technology, Suzhou 215500, China
[2]Department of Electrical and Computer Engineering, Dalhousie University, Halifax, NS B3H 4R2, Canada
[3]School of Information Science and Engineering, East China University of Science and Technology, Shanghai 200237, China
[4]East China University of Science and Technology, Research Institute of Changshu Company Ltd., Suzhou 215500, China
[5]College of Electrical and Information Engineering, Lanzhou University of Technology, Lanzhou 730000, China

Corresponding author: Jason Gu (Jason.gu@dal.ca)

This work was supported in part by the Natural Science Foundation of Jiangsu Province under Grant BK20170436 and Grant BK20181033, in part by the Jiangsu Postdoctoral Research Project, in part by the State Scholarship Fund Organized by China Scholarship Council, in part by the National Natural Science Foundation of China under Grant 61901062 and Grant 61903050, and in part by the National Science and Engineering Research Council of Canada.

ABSTRACT Bradycardia and tachycardia reflect abnormalities of the heart that can lead to severe harm to the cardiovascular system. The pulsatile signal is a useful tool to detect these two kinds of arrhythmias. In this study, we present a pulsatile synthesis-by-analysis (PSA) modeling based method to detect bradycardia and tachycardia. A new PSA modeling method was proposed to quantitively describe the changes of pulsatile waves, and we obtained twelve parameters for constructing a feature vector from the PSA model of each wave, by which we trained classifiers of probabilistic neural network (PNN) and random forest (RF). Our experiments were performed on the Fantasia and 2015 PhysioNet/CinC Challenge databases. Some pathological and physiological changes were extracted from the average models of the subjects in different groups. The two-sample *ks*-test results show that all the parameters between different groups are all markedly different ($h = 1, p < 0.05$). The classification results show that the performances of RF classifiers are better than that of PNN. The kappa coefficients (KC) of RF classifiers are all over 97%, and that of the classifying among bradycardia, tachycardia, and healthy subjects is $98.652 \pm 0.217\%$. Compared with the performance of some former methods, the obtained results demonstrate that the presented method promotes the classification performance remarkably and has the potential to diagnose bradycardia and tachycardia in m-health.

INDEX TERMS Synthesis-by-analysis modeling, pulsatile signal, bradycardia and tachycardia detection, random forest.

I. INTRODUCTION

Bradycardia and tachycardia, two critical symptoms of some cardiovascular diseases (CVDs), have caught the attention of many researchers in recent years. With the continuous degradation of heart function, these two arrhythmias may deteriorate into two life-threatening malignant arrhythmias, the extreme bradycardia (EB) with the heart rate lower than 40 beats per minute (bpm) for 5 consecutive beats, and the extreme tachycardia (ET) with the heart rate higher than 140 bpm for 17 consecutive beats [1]. They may lead to acute CVDs, such as sudden cardiac death [2]. However, the bradycardia and tachycardia outburst and recover within a short time, thus they are easy to be ignored by patients and doctors [3]. Since diagnosis in the hospital is limited, it is important to accurately detect bradycardia and tachycardia in daily life before they deteriorate into EB and ET.

Electrocardiogram (ECG) plays an important role in the diagnosis of CVDs, some indexes extracted from its morphology (R wave [4], QRS complexes [5], T wave, P wave [6], U wave [7], approximate entropy [8]) or/and heartbeat intervals (HBIs) (heart rate [9], heart rate variability [10], heart

The associate editor coordinating the review of this manuscript and approving it for publication was Nuno Garcia.

rate turbulence [11], deceleration capacity [12]) are effective in identifying and predicting some life-threatening arrhythmias. Hammad *et al.* [13] extracted 13 features from ECG to detect the abnormal heart conditions with the highest average accuracy of 99%. They also proposed a deep features extraction framework for arrhythmia detection and biometric authentication [14], [15]. Li et al. abstracted some nonlinear features from ECG with wavelet packet decomposition [16] or kernel independent component analysis [17] for arrhythmia classification and obtained a high accuracy of over 97%. These ECG-based studies have proven effective in arrhythmias detection. However, the multiple electrode attachments and cable connections required in ECG recording limit the portability of ECG-based devices, the long-time attached electrodes would cause skin allergies, and the data recording needs the help of a doctor or nurse, which limits the application of relevant results in m-health or telemedicine.

Heartbeat creates a change in the voltage difference across the surface of the skin. This change, recorded by electrode attachments, is the ECG signal. As the heart beats, blood vessels fill and blood circulates, relaying information about hemodynamics and heart rhythm to distal vessels. We can record this information through pulsatile sensors placed on the wrist [18], the fingertips [19], the ear [20] and other parts of the body [21]. Many studies have demonstrated that the pulse beat intervals (PBIs) extracted from the pulsatile signal, e.g., photoplethysmogram (PPG) or arterial blood pressure (ABP), an be a substitute for HBIs to detect CVDs such as arrhythmia [22], hypertension [23] and coronary heart disease [24]. Compared to the ECG recording process, the pulsatile signal recording requires only one sensor without the help of nurses or doctors. As such, it has become a research hotspot for wearable health monitoring devices such as smartwatches, bracelets, rings, and earplugs [21]. The pulsatile signal has potential in detecting and predicting bradycardia and tachycardia in m-health.

PBIs and derived parameters are employed to describe the rhythm of the cardiovascular system or to detect these arrhythmias. Hochstadt *et al.* [25] concluded that the PBIs have the same function in monitoring atrial fibrillation (AF) as the HBIs. Gil *et al.* [26] extracted the pulse rate turbulence from PBIs to identify ventricular premature. Lee *et al.* [27] used the root-mean-square of the successive differences (RMSSD) and the Shannon entropy (ShE) of PBIs to classify the obtained PPG signals into AF and normal sinus rhythm with the highest accuracy of 99.32%. While these studies focused on PBIs and the pathological role in heartbeat rhythm and ignored the changes in hemodynamics, they achieved good results in detecting arrhythmias.

In addition, some researchers have noticed that the arrhythmias can cause variations in the pulsatile waveform, and the variations are related to the change of hemodynamics. Thus, the PBIs-based and wave-based features were engaged to detect some arrhythmias. The root-mean-square and Poincare-plot' ShE of the PBIs, and the pulse rise and fall times were exploited to discriminate normal sinus rhythm, AF, premature ventricular contractions and premature atrial contraction in [28], and the sensitivity, the specificity, and the accuracy of the classifications are all over 96%. In [29], ten statistical parameters of the PBIs and six wave-based features (adaptive organization index, the variance of the slope of the phase difference, permutation entropy, spectral entropy, fractional spectral radius, and spectral purity index) were used to discriminate between AF and ventricular arrhythmias. The experimental results indicate that the classifying performance of wave-based features is better than that of PBIs-based features. The contribution of these studies is to prove it is feasible to detect arrhythmias using the pulsatile signal. Studies have achieved good experimental results with the wave-based and PBIs-based features, while the physiological or pathological implications of these features require further investigation. Although these methods have not been used to detect bradycardia and tachycardia, they provide a framework for related studies.

As the heart contracts, blood is squeezed from the left ventricle into the aorta and travels down the systemic vascular network. Then, the blood is reflected in the junctures between the thoracic and abdominal aorta and the junctures between the abdominal aorta and common iliac arteries, and reflected again in distal vascular structure because of the considerable variation in arterial resistance and compliance. As a result, the pulsatile signal we recorded consists of a pressure wave and several reflection waves [30]. According to this physiological process, a method called pulsatile synthesis-by-analysis (PSA) has been proposed to model the pulsatile wave, and several kernel functions have been utilized to simulate the pressure and refection waves [31]. So far, related works focus on the study of the number and types of kernel functions, and the model expression. The Gaussian, Lognormal, Rayleigh, Gamma [32], double-exponential [33] and cosine [34] functions are used as the kernel functions in past studies. The number of kernel functions used in modeling varies from one up to seven [32], [35]. The model can be synthesized by several single-kernel functions or a mixture of several kernel functions. One to six Gaussian, Lognormal, Rayleigh or Gamma functions in [32], seven Gaussian functions in [35], one Lognormal and two Gaussian functions, one Gamma and two Gaussian functions in [36], one Gamma and four Gaussian in [37], and two Gaussian and three cosine functions in [38] and [39]. There is controversy over the model of the pulsatile wave. Recently, Jiang *et al.* [33], [40] suggested that the ABP wave can be accurately synthesized by three Gaussian or three Lognormal functions.

The PSA method has been used for signal compression [35], abnormal segments detection and reconstruction [41], [42] and physiological and pathological information mining of cardiovascular system [30] since it was proposed. The pressure and reflection waves carry much information about the cardiovascular system, so some cardiac function and hemodynamics related parameters such as augmentation index, stiffness index, reflection index, crest time, left ventricular ejection time, pulse pressure and vascular tone,

are derived using PSA modeling methods. These parameters have been exploited to detect arterial stiffness [43], coronary artery disease [44], AF [36], arterial blood pressure [45], heart failure [46]. These works indicate that the PSA models can quantitatively describe the changes in pulsatile waveform and are effective in detecting some cardiovascular diseases. Potential for bradycardia and tachycardia detection still needs to be explored.

Bradycardia and tachycardia alter pulse beat rhythm and hemodynamic parameters of patients, but the existing methods pay more attention to beat rhythm while ignoring hemodynamics. Thus, a new PSA modeling method is proposed in this study to detect the bradycardia and tachycardia and to quantitatively describe the changes of pulsatile signal and their corresponding implications of beat rhythm and hemodynamics caused by these two arrhythmias. First, the noise and interference are filtered out, and the abnormal segments are recognized and removed from the pulsatile signal. Then, combing the PBIs, the baseline and the shape of the pulsatile waves, a novel PSA modeling method is proposed, and the average models of healthy subjects, bradycardia and tachycardia subjects are obtained from measured data. Next the physiological and pathological variations caused by bradycardia and tachycardia are extracted from these models, and the markedly changed model parameters are employed as the feature vector to train the classifiers of probabilistic neural network (PNN) and random forest (RF) for detecting the bradycardia and tachycardia. The data of Fantasia and the PhysioNet/Computing in Cardiology Challenge 2015 database are used to validate our method.

The remainder of the paper is organized as follows. The database and the proposed method are described in detail in section II. The main results are presented and discussed in section III and IV. Finally, the conclusion is given in section V.

II. MATERIALS AND METHODS

A. EXPERIMENTAL DATA

The experimental data consists of two sets, both from the international physiological signal database: *PhysioBank*. A set of data is recorded from healthy subjects and the other set is from the subjects with bradycardia and tachycardia.

The data of healthy subjects are from Fantasia database [47] which supplies data of 10 healthy young (21 - 31 years old) and 10 elderly (70 - 85 years old) rigorously-screened subjects in sinus rhythm. The numbers of male and female is equal. See Table 1. All subjects underwent a physical examination, routine blood count and biochemical test before the experiment, and only healthy, nonsmoking subjects were engaged. The continuous ECG, respiration and ABP signals were collected for each subject who remained in a lay-supine state watching the 1940 Disney movie *Fantasia* to help maintain wakefulness. The sampling frequency of each signal was 250 Hz and its length was 120 minutes. The names of records are f2y01m - f2y10m and f2o01m - f2o10m for the young and elderly subjects, respectively.

TABLE 1. The information about the subjects in the fantasia database.

Name of Records	Age	Sex	Name of Records	Age	Sex
f2o01m	73	Female	f2y01m	23	Female
f2o02m	75	Female	f2y02m	23	Male
f2o03m	85	Female	f2y03m	28	Female
f2o04m	70	Female	f2y04m	27	Female
f2o05m	83	Male	f2y05m	25	Female
f2o06m	70	Male	f2y06m	26	Male
f2o07m	77	Male	f2y07m	31	Male
f2o08m	71	Male	f2y08m	21	Male
f2o09m	77	Male	f2y09m	21	Female
f2o10m	73	Female	f2y10m	21	Male

The data of bradycardia and tachycardia subjects are from the database of 2015 PhysioNet/CinC Challenge [48], in which the data of five life-threatening arrhythmias (asystole, EB, ET, ventricular tachycardia, and ventricular flutter/fibrillation) are supplied to encourage the development of some methods to reduce the incidence of false alarms in the intensive care unit. The data were recorded in four hospitals in the USA and Europe using the monitoring equipment of three major manufacturers. To supply a "gold standard" list of true and false alarms, a team of experts visually inspected the waveform record extensively. Each annotator worked independently and was assigned a randomized list of patients to review. In order to ensure the accuracy of annotation, the data were independently reviewed by at least two annotators, of whom, a two-thirds majority had to agree that the alarm was either True or False. Here, the data of the subjects with EB and ET are engaged in this study. Because some of the data are corrupted by movement artifact, sensor disconnects, and other events, the data of seventeen bradycardia subjects (records name: b268s, b455l, b456s, b494s, b495l, b515l, b516s, b517l, b560s, b561l, b562s, b578s, b659l, b664s, b708s, b722s and b757l) and twenty-three tachycardia subjects (records name: t173l, t208s, t214s, t276s, t277l, t333l, t335l, t406s, t412s, t413l, t417l, t418s, t425l, t594s, t677l, t680s, t690s, t702s, t707l, t719l, t739l, t760s and t777l) are chosen. Each record contains two ECG and one ABP signal with a length of 5 minutes or 5.5 minutes and with the sampling frequency of 250 Hz.

B. THE THEORY OF PULSATILE SYNTHESIS-BY-ANALYSIS MODELING METHOD

A cardiac cycle results from systole and diastole of the heart and corresponds to a cycle in the pulsatile signal, as shown in Fig. 1. The i-th pulsatile wave is denoted as $y_i(n)$, $i \in [1, M]$, M is the number of waves in the pulsatile signal, n is the n-th samples in $y_i(n)$, $n \in [1, PPI(i)]$. $PPI(i)$ is the i-th pulsatile beat interval (PBI) and can be calculated by:

$$PPI(i) = PW(i) - PW(i-1) \tag{1}$$

where $PW(i)$ and $PW(i-1)$ are the start and end of $y_i(n)$.

Thus, the pulsatile rate (PR) is:

$$PR(i) = 60 \times f_s / PPI(i) \tag{2}$$

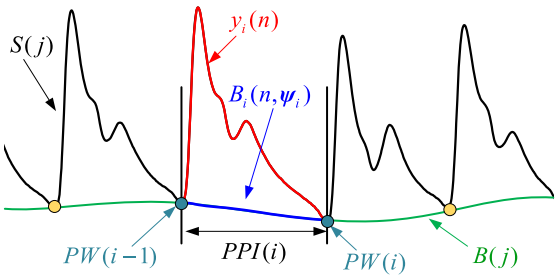

FIGURE 1. Composition of pulsatile signal in the time-space domain.

where f_s is the sampling frequency. It has been confirmed that the sequences of PBI or PR contain abundant physiological and pathological information about the cardiovascular system and autonomic nervous system [49], [50] and have been employed to classify some arrhythmias [28], [29], [51].

If the pulsatile signal is denoted as $S(j), j \in [1, L]$, L is the length of a signal. Then:

$$S(j) = \{y_i(n)\}_{i=1}^{M} \tag{3}$$

which means a pulsatile signal is connected by the M waves in the time domain in the order of $\{PW(i)\}_{i=1}^{M}$.

In Fig. 1, the amplitudes of the start and end of each pulsatile wave change slightly, then we can see a baseline of pulsatile signal (the green curve) after interpolating. We denote it as $B(j)$. It is unknown whether the baseline contains some physiological or pathological information, thus, the baseline is integrated into the PSA model:

$$\hat{y}_i(n) = \boldsymbol{f}(n, \boldsymbol{\theta}_i) + B(n, \boldsymbol{\psi}_i) \quad n \in [1, PPI(i) + 1] \tag{4}$$

where, $\hat{y}_i(n)$ is the estimated value of n-th sample in i-th pulsatile wave. The first term on the right side of the equation is the spatial expression of the pulsatile wave, and the second term is the expression of the baseline. $\boldsymbol{f}(\cdot)$ represents a combination of one or several kernel functions. $\boldsymbol{\theta}_i$ and $\boldsymbol{\psi}_i$ are the parameter vectors of the i-th pulsatile model.

For (4), we need to further obtain a detailed expression. For $\boldsymbol{f}(n, \boldsymbol{\theta}_i)$, Tigges *et al.* [52] concluded that the pulsatile wave can be fitted under an arbitrarily small error by increasing the number of kernel functions, but it may lead to overfitting and result in some physiologically unexplained results. Additionally, Nosrati and Tavassolian [53] found that the heartbeat motion of the chest wall is pulsatile rather than a simple sinusoidal. The research results of [33] suggested that three positive Gaussian functions can accurately synthesize the pulsatile wave. For $B(n, \boldsymbol{\psi}_i)$, because the baseline in a cardiac cycle can be approximated as a straight line segment, here, it is described by a linear function. Thus, (4) is:

$$\begin{aligned}\hat{y}_i(n) &= \boldsymbol{f}(n, \boldsymbol{\theta}_i) + B(n, \boldsymbol{\psi}_i) \\ &= \sum_{l=1}^{3} f_i^l(n, a_i^l, b_i^l, c_i^l) + k_i n + b_i \\ &= \sum_{l=1}^{3} a_i^l \exp[-\frac{(n - b_i^l)^2}{(c_i^l)^2}] + k_i n + b_i \quad n \in [1, PPI(i)]\end{aligned} \tag{5}$$

where, $f_i^l(n, a_i^l, b_i^l, c_i^l)$ is the l-th kernel function of the i-th pulsatile wave model, f_i^1, f_i^2 and f_i^3 represent the systolic wave, incisura wave and dicrotic wave of a typical single-period pulsatile wave, respectively. a_i^l, b_i^l and c_i^l are the height, the position and the width of the l-th Gaussian function. $k_i n + b_i$ is the expression of the baseline, k_i is the slope, and b_i is the vertical intercept. Fig. 2 illustrates a pulsatile wave model.

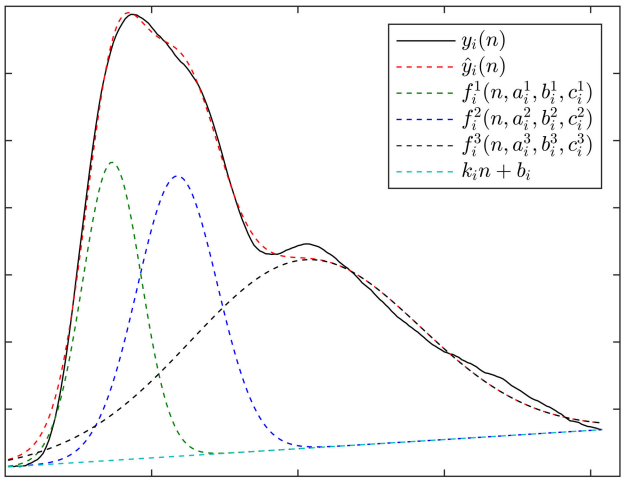

FIGURE 2. Composition of a pulsatile wave model.

Thus, the i-th pulsatile wave can be quantified by the following parameters:

$$\begin{aligned}\boldsymbol{P}_i &= [\,PPI(i)\;\; \boldsymbol{\psi}_i\;\; \boldsymbol{\theta}_i\,] \\ &= [\,PPI(i)\;\; k_i\;\; b_i\;\; a_i^1\;\; b_i^1\;\; c_i^1\;\; a_i^2\;\; b_i^2\;\; c_i^2\;\; a_i^3\;\; b_i^3\;\; c_i^3\,]\end{aligned} \tag{6}$$

where, $\boldsymbol{\psi}_i = [\,k_i\;\; b_i\,]$, $\boldsymbol{\theta}_i = [\,a_i^1\;\; b_i^1\;\; c_i^1\;\; a_i^2\;\; b_i^2\;\; c_i^2\;\; a_i^3\;\; b_i^3\;\; c_i^3\,]$.

Then, we can get a vector constructed by all the pulsatile waves of a pulsatile signal:

$$\begin{aligned}\boldsymbol{P} &= [\,\boldsymbol{PPI}\;\; \boldsymbol{\psi}\;\; \boldsymbol{\theta}\,] \\ &= [\,\boldsymbol{PPI}\;\; \boldsymbol{K}\;\; \boldsymbol{B}\;\; \boldsymbol{A}^1\;\; \boldsymbol{B}^1\;\; \boldsymbol{C}^1\;\; \boldsymbol{A}^2\;\; \boldsymbol{B}^2\;\; \boldsymbol{C}^2\;\; \boldsymbol{A}^3\;\; \boldsymbol{B}^3\;\; \boldsymbol{C}^3\,]\end{aligned} \tag{7}$$

C. PROCESS OF BRADYCARDIA AND TACHYCARDIA DETECTION

The process of bradycardia and tachycardia detection includes: 1) pulsatile signal pre-processing, 2) obtaining the feature vector from the PSA model, 3) bradycardia and tachycardia detecting, as shown in Fig. 3. In signal pre-processing, the noise and interference in pulsatile signals are attenuated, the abnormal segments are detected and wiped out, and the start points of pulsatile waves are identified and engaged to split a signal into a series of waves by pulsatile beat. Then, the PSA model parameters of each pulsatile wave are calculated or estimated to generate the feature vector. The features of different subjects are divided into training and testing sets, by which we train the classifier and test the classifying results.

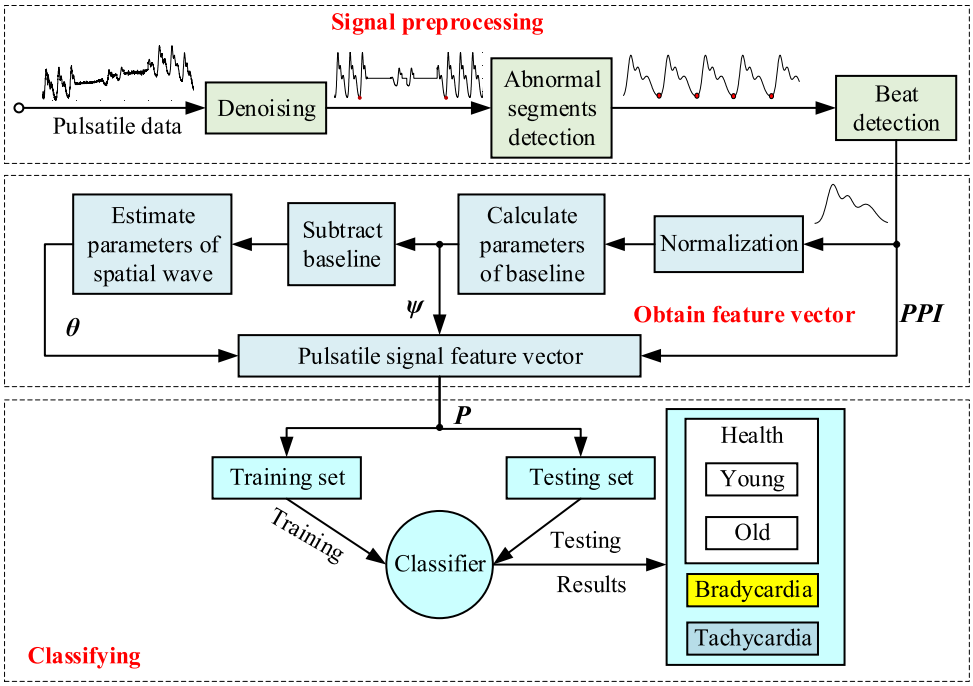

FIGURE 3. Overview of the proposed method.

1) PULSATILE SIGNAL PREPROCESSING

The measured pulsatile signal contains some noise and interference, i.e., DC component, baseline wanders, power line interference and muscle contraction. Here, a modified mathematical morphology filtering method is employed to eliminate noise and interference [54]. The symmetric structuring element is a line segment with an amplitude of 20. First, an alternate-hybrid filter, whose symmetric structuring element's length is 10 samples, is designed to eliminate power line interference and muscle contraction. The results are denoted as $\{S_1(j)\}$. Next, we increase the symmetric structuring element's length up to 200 samples for another alternate-hybrid filter which is employed to estimate the tendency of DC component and baseline wanders. Results are denoted as $\{C(j)\}$. Then, we obtain the filtering result by $\{S_1(j)\}$ - $\{C(j)\}$.

Some abnormal segments caused by movement artifact, sensor disconnects or movement, and other events still exist in pulsatile signal even after denoising. These segments lose some of or almost all the waveform characteristics and have a great influence on the accuracy of beat detection. Thus, they should be detected and wiped out from the pulsatile signal. Here, we use an ASCD method to detect the abnormal segments [55]. Then, the clear pulsatile signal $\{S(j)\}$ is obtained.

For the pulsatile wave segmentation, we find the start points of each pulsatile wave. Because the peak of systolic wave is the most prominent feature in a pulsatile wave, and the start point is the minimum between two adjacent systolic waves, here, we first compute the PBIs using a sliding window iterative method [34]. The start point is located in the minimum of waveform in each PBI. The pulsatile waves are denoted as $\{x_i(n)\}_{i=1}^{M}$, and we can obtain the feature $PPI(i)$ using the start points $\{PW(i)\}_{i=1}^{M}$ according to (1).

2) OBTAINING FEATURE VECTOR FROM PSA MODEL

After obtaining pulsatile waves, we compute the parameters of the PSA model. Fig. 3 shows the process. There are four steps: a) normalization, b) calculate the parameters of baseline, c) subtract baseline from pulsatile wave, and d) estimate parameters of the spatial wave.

The pulsatile waves are normalized by:

$$y_i(n) = \frac{x_i(n) - \frac{1}{PPI(i)} \sum_{n=1}^{PPI(i)} x_i(n)}{\sqrt{\frac{1}{PPI(i)} \sum_{n=1}^{PPI(i)} \left(x_i(n) - \frac{1}{PPI(i)} \sum_{n=1}^{PPI(i)} x_i(n) \right)^2}} \tag{8}$$

where $y_i(n)$ is the result of n-th samples in i-th pulsatile wave.

For the i-th pulsatile wave after normalizing, the parameters of its baseline can be calculated by:

$$k_i = \frac{y_i(PPI(i)) - y_i(1)}{PPI(i) - 1} \tag{9}$$

$$b_i = y_i(1) - k_i \tag{10}$$

where $y_i(1)$ and $y_i(PPI(i))$ are the start and end of the pulsatile wave.

In (5), the Gaussian functions in the PSA model are limited by the Dirichlet and Neumann boundary conditions [23]:

$$\lim_{n \to -\infty} f(n) = \lim_{n \to \infty} f(n) = 0 \tag{11}$$

$$\lim_{n \to -\infty} [f(n) - f(n-1)] = \lim_{n \to \infty} [f(n) - f(n-1)] = 0 \tag{12}$$

The normalized pulsatile wave does not satisfy this condition, as shown in Fig. 1. However, we find the waveform obtained by subtracting the baseline from the pulsatile wave, whose amplitudes of the start and end points are 0, and approximate these conditions. The result is denoted as $z_i(n)$, so:

$$z_i(n) = y_i(n) - k_i n - b_i \tag{13}$$

where, $z_i(n)$ is the spatial wave and can be used to estimate the parameters of $\boldsymbol{f}(n, \boldsymbol{\theta}_i)$ in (5) by curve fitting. The fitting error is defined as:

$$E_i(\boldsymbol{\theta}_i) = \frac{1}{PPI(i)} \sum_{n=1}^{PPI(i)} (z_i(n) - \boldsymbol{f}(n, \boldsymbol{\theta}_i))^2 \tag{14}$$

Then, we can obtain the optimal parameters by:

$$\begin{aligned} &\min_{\boldsymbol{\theta}_i} E_i(\boldsymbol{\theta}_i) \\ &\text{subject to } \boldsymbol{F}\{\boldsymbol{f}(n, \boldsymbol{\theta}_i), \boldsymbol{\theta}_i\} \quad \text{and } lb \le \boldsymbol{\theta}_i \le ub \end{aligned} \tag{15}$$

where, $\boldsymbol{F}\{\boldsymbol{f}(n, \boldsymbol{\theta}_i), \boldsymbol{\theta}_i\}$ and $lb \le \boldsymbol{\theta}_i \le ub$ are the constraints and boundary conditions of parameters, respectively. lb and ub are the lower and upper bounds. Here, the nonlinear least-squares method is engaged to solve (15). The optimization algorithm, constraints and boundary conditions we selected are shown in Table 2.

TABLE 2. Parameters setting of curve fitting.

Parameters	Values
lb	$[\min(z_i(n)),\ 0,\ 0,\ \min(z_i(n)),\ 0,\ 0,\ \min(z_i(n)),\ 0,\ 0]$ [a]
ub	$[\max(z_i(n)),\ 0.5PPI(i),\ PPI(i),\ \max(z_i(n)),\ 0.8PPI(i),\ PPI(i)\ \max(z_i(n)),\ PPI(i),\ PPI(i)]$
$\boldsymbol{F}\{\boldsymbol{f}(n, \boldsymbol{\theta}_i), \boldsymbol{\theta}_i\}$	$a_i^1 > a_i^3, a_i^2 > a_i^3, b_i^1 < b_i^2 < b_i^3$
Intitial values	[2.919 0.107 0.043 2.086 0.205 0.046 1.580 0.343 0.050]
Optimization algorithm	'Trust-Region'
Maximum number of iterations	400
Iterative termination condition	$E_i(\boldsymbol{\theta}_i) \le 0.010$

[a] $\min(z_i(n))$ and $\max(z_i(n))$ are the minimum and maximum of the i-th pulsatile wave, respectively.

3) BRADYCARDIA AND TACHYCARDIA DETECTING

For the data in the Fantasia database, the number of pulsatile waves obtained is 41770 for young subjects, 38140 for elderly subjects, and thus 79310 for healthy subjects in total. Then for the data in the 2015 PhysioNet/CinC Challenge database, the number of pulsatile waves extracted are 4595 for bradycardia and 12089 for tachycardia. A feature vector contains twelve parameters for each pulsatile wave, and we have a 95994×12 feature vector to train and test classifiers. Then, we train the classifiers to detect which groups the pulsatile waves come from. The numbers of training and testing sets are shown in Table 3, and the data from different groups are labeled with different numbers for classification. In addition, we do not do cross-validation in training classifiers.

TABLE 3. The training set and testing set of different classifications.

Classification[a]	Training Set	Testing Set	Total	Labels
Y vs O	71310	8000	79310	1 vs 2
Ht vs Bc	75905	8000	83905	1 vs 2
Ht vs Tc	83399	8000	91399	1 vs 2
Bc vs Tc	14684	2000	16684	1 vs 2
Ht vs Bc vs Tc	87994	8000	95994	1 vs 2 vs 3

[a] Here, the 'Y', 'O', 'Ht', 'Bc' and 'Tc' are the abbreviations of young, old, healthy, bradycardia and tachycardia subjects, respectively.

The classifiers designed methods we used in this study are PNN and RF. The neural network toolbox in MATLAB 2016a is employed to construct the PNN classifier. PNN is a kind of radial basis network suitable for classification. Here, the function 'newpnn($\boldsymbol{P}$, $\boldsymbol{T}$, *spread*)' in the toolbox is utilized to create a two-layer network, $\boldsymbol{P}$ is the input vectors, $\boldsymbol{T}$ is the target class vectors, *spread* is the spread of radial basis functions (RBF). The first layer consists of RBF neurons and their weighted inputs are computed with Euclidean distance weight function. The second layer has competitive transfer function neurons and their weighted inputs are calculated with Dot product weight function. The spread speed we used is 0.02.

RF is a machine learning method which adds an additional layer of randomness to bagging on the basis of the decision tree method. The Gini index is used to generate the thresholds. The function 'classRF_train($\boldsymbol{P}$, $\boldsymbol{T}$, *ntree*, *mtry*, *extra_options*)' in the open-source toolbox 'randomforest-matlab' [56] (available at https://code.google.com/archive/p/randomforest-matlab/) is engaged to train RF classifiers. $\boldsymbol{P}$ and $\boldsymbol{T}$ are the input vectors and the target class vectors, *ntree* is the number of trees grown and is set to 10, *mtry* is the number of predictors sampled for splitting at each node and can be calculated by the number of features (here we use 3), *extra_options* is other options to control RF and their initial values are the default.

III. RESULTS

In this study, the specificity (Sp), sensitivity (Se) and accuracy (Ac) are defined to assess the classifying results:

$$Sp = \frac{TN}{FP + TN} \times 100\% \tag{16}$$

$$Se = \frac{TP}{TP + FN} \times 100\% \tag{17}$$

$$Ac = \frac{TP + TN}{TP + FP + FN + TN} \times 100\% \tag{18}$$

where, TP (True Positive) means the pulsatile wave belongs to A and is classified as A. FP (False Positive) means the pulsatile wave belongs to B and is classified as A. FN (False Negative) means the pulsatile wave belongs to A and is classified as B. TN (True Negative) means the pulsatile wave belongs to B and is classified as B. Here, A and B represent which category the pulsatile wave belongs to. For the classification of the young and elderly subjects, B is the elderly subject and A is the young subject. For the classification between

healthy subjects and unhealthy subjects, A is the subject with bradycardia or tachycardia, and B is healthy subject consist of young and older. For classification of unhealthy subjects, A is the bradycardia subject and B is the tachycardia subject.

The three indexes we defined above can only assess part of the performance of classifiers, so to complement, the kappa coefficient (KC) is exploited to measure their average performance [57], [58]:

$$KC = \frac{p_0 - p_e}{1 - p_e} \tag{19}$$

$$p_0 = \frac{\sum_{t=1}^{r} q_{tt}}{m} \tag{20}$$

$$p_e = \frac{\sum_{t=1}^{r} (q_{t+} \times q_{+t})}{m^2} \tag{21}$$

where, the p_0 and p_e can be derived from the contingency matrix of the classification results. q_{tt} is the element on the diagonal of the contingency matrix, q_{t+} is the sum of the elements on the line t, and q_{+t} is the sum of the elements on the column t. m is the number of pulsatile waves that need to be classified, r is the number of the rows or columns of contingency matrix. $KC \in [-1, 1]$, and the closer the value of KC is up to 1, the better the classification result. Then, the assessment indicator for each category is defined as:

$$KC_t = \frac{p_{tt} - p_{t+}p_{+t}}{p_{+t} - p_{t+}p_{+t}} \tag{22}$$

$$p_{tt} = \frac{q_{tt}}{m} \tag{23}$$

$$p_{t+} = \frac{q_{t+}}{m} \tag{24}$$

$$p_{+t} = \frac{q_{+t}}{m} \tag{25}$$

The simulated software used is MATLAB 2016a which is installed at a laptop with an Intel(R) Core (TM) i7-6700HQ CPU @ 2.6 GHz, windows-7 64-bit operating system and installed memory of 16 GB.

A. ARESULTS OF PSA MODELING

The pulsatile waveforms of healthy and unhealthy subjects are utilized to estimate the parameters of PSA models by curve fitting. The results are shown in Table 4. Then, the means of these parameters are substituted into (5), and the average PSA models of different groups are obtained, as shown in Fig. 4 and Fig. 5.

For the models of the young and elderly subjects, we conclude that:

a) The heart rate slows down with aging. In Table 4, the average ***PPI*** increases from 0.928 s to 1.024 s, which corresponds to the widening of the model in Fig. 4.

b) The contractility of the heart weakens with aging. In Table 4, the average of $\boldsymbol{A}^1$ decreases from 3.105 to 2.241, which corresponds to the amplitude's changing of $\overline{f^1}$ in Fig. 4. f^1 is the systolic wave generated by contracting of the heart. The higher the wave peak, the stronger the heart's ability to contract.

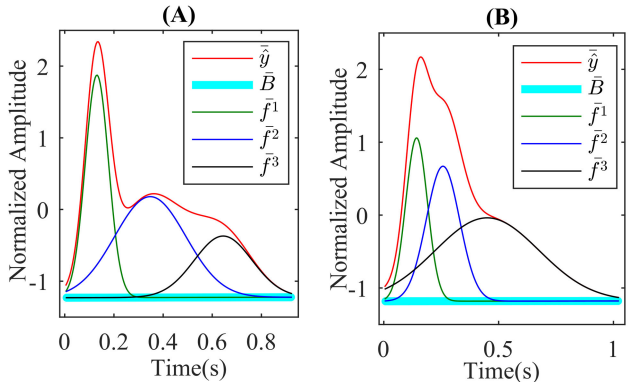

FIGURE 4. The average PSA models for young (A) and older (B). The overline above the variables indicates their average.

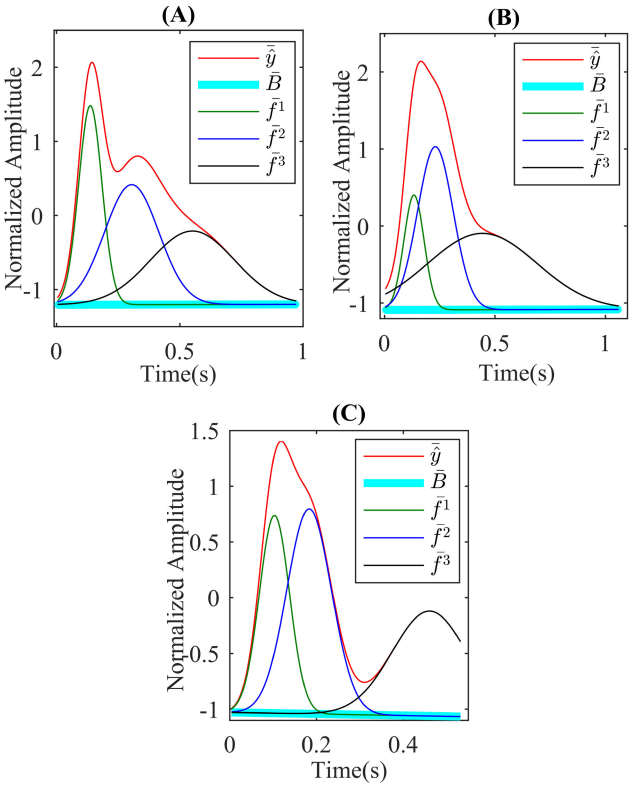

FIGURE 5. The average PSA models for healthy subjects (A), subjects with bradycardia (B) and tachycardia (C).

c) The arterial elasticity decreases with aging. In Table 4, the average of $\boldsymbol{B}^2$ reduces from 0.348 s to 0.258 s, and that of $\boldsymbol{B}^3$ reduces from 0.644 s to 0.450 s, which corresponds to the narrowing of $\overline{f^2}$ and $\overline{f^3}$, respectively. These two reflected waves are generated from vasoconstriction, which causes blood to flow back. The closer f^2 and f^3 are to f^1, the faster the blood reflux speed, and the smaller the blood vessel deformation; that is, the degree of arterial stiffness increases and the elasticity decreases. Moreover, the values of $\boldsymbol{A}^2$ and $\boldsymbol{A}^3$ increase with aging, which indicates that the volume of the blood flowing back decreases, by which we can also infer that the elasticity of the blood vessel reduces.

For comparing the models between the healthy subjects and the unhealthy subjects, here, the pulsatile waves of the young and elderly subjects are mixed to generate the health PSA model by (5). Then, we can obtain some conclusions from the PSA models of healthy subjects and unhealthy subjects with bradycardia and tachycardia as follow:

a) The heart rate of healthy subjects is higher than that of bradycardia subjects and lower than that of tachycardia subjects. In Table 4, the average ***PPI*** for healthy subjects is 0.974 s, while that of bradycardia and tachycardia subjects are 1.064 s and 0.542 s, respectively. Their corresponding heart rates are 61.457 bpm, 56.391 bpm, and 110.701 bpm.

TABLE 4. The parameters of PSA models for different subjects. Data are expressed as mean ±SD.

P	Young	Old	Health	Bradycardia	Tachycardia
A^1	3.105±0.540	2.241±0.592	2.689±0.711	1.492±0.743	1.774±0.831
B^1	0.131±0.112	0.143±0.039	0.137±0.085	0.133±0.076	0.103±0.080
C^1	0.067±0.034	0.068±0.017	0.067±0.027	0.065±0.029	0.049±0.029
A^2	1.408±0.419	1.852±0.358	1.621±0.449	2.119±0.375	1.838±0.727
B^2	0.348±0.149	0.258±0.098	0.305±0.134	0.230±0.079	0.183±0.080
C^2	0.205±0.113	0.102±0.057	0.156±0.104	0.114±0.079	0.073±0.023
A^3	0.856±0.628	1.143±0.275	0.994±0.511	0.992±0.286	0.941±0.906
B^3	0.644±0.703	0.450±0.071	0.551±0.518	0.442±0.186	0.461±0.536
C^3	0.166±0.161	0.321±0.095	0.240±0.154	0.350±0.224	0.122±0.170
K	0.007±0.176	0.004±0.200	0.006±0.188	0.007±0.201	-0.070±1.206
B	-1.231±0.180	-1.182±0.204	-1.207±0.193	-1.090±0.200	-1.029±0.437
PPI	0.928±0.204	1.024±0.181	0.974±0.199	1.064±0.469	0.542±0.886

b) The cardiac contractility of healthy subjects is stronger than that of unhealthy subjects. From Fig. 5, the amplitude of f^1 for healthy subjects is 2.689, which is obviously higher than that of unhealthy subjects (bradycardia: 1.492, tachycardia: 1.774). This indicates that the cardiac contractility of the healthy subjects is strongest, followed by the tachycardia subjects, and the weakest for the bradycardia subjects.

c) The arterial contractility of healthy subjects is stronger than that of unhealthy subjects. The relative positions of f^2 to f^1 for bradycardia and tachycardia subjects are 0.097 s and 0.080 s, while that of healthy subjects is 0.168 s. Thus, the arterial contractility of the healthy subjects is strongest, followed by the bradycardia subjects, and weakest for the tachycardia subjects.

d) The cardiac contraction speed is noticeably accelerated for tachycardia subjects. In Fig. 5, the relative position of the second reflected wave is obviously delayed, which indicates the dysfunction of heartbeat, e.g., a new cardiac contraction starts during the last diastole period.

B. CLASSIFICATION RESULTS

The two-sample Kolmogorov-Smirnov test (*ks*-test) is employed to select the parameters of PSA models between subjects in two different groups for classifying. The results are shown in Table 5. Here, the null hypothesis is that the samples of two different sets obey the same probability distribution. The result h is 1 if the test rejects the null hypothesis at the 5% significance level, and 0 otherwise. Thus,

TABLE 5. The results of *ks*-test for different subjects. '*h*' and '*p*' are the hypothesis and probability of *ks*-test.

P	Y vs O		Ht vs Tc		Ht vs Bc		Tc vs Bc	
	h	p	h	p	h	p	h	p
A_1	1	0	1	0	1	0	1	6.977×10^{-146}
B_1	1	0	1	0	1	3.334×10^{-114}	1	9.098×10^{-143}
C_1	1	7.651×10^{-218}	1	0	1	1.775×10^{-171}	1	0
A_2	1	0	1	0	1	0	1	0
B_2	1	0	1	0	1	0	1	0
C_2	1	0	1	0	1	9.974×10^{-304}	1	0
A_3	1	0	1	0	1	8.576×10^{-120}	1	0
B_3	1	0	1	0	1	1.528×10^{-124}	1	0
C_3	1	0	1	0	1	1.859×10^{-251}	1	0
K	1	1.231×10^{-312}	1	0	1	4.372×10^{-4}	1	0
B	1	0	1	0	1	0	1	1.918×10^{-215}
PPI	1	0	1	0	1	1.205×10^{-321}	1	0

the two-sample *ks*-test results demonstrate that the parameters obtained are all markedly different ($h = 1, p < 0.05$). Then, these parameters are employed to train the different classifiers for classifying pulsatile waves of different groups.

The PNN and RF methods are exploited to classify the pulsatile waves by their PSA model parameters for the subjects in different groups. In order to eliminate the influence of the different input samples on classifying results, we randomly change the samples in the training set and testing set while keeping their number unchanged, and run the program 100 times. Results are shown in Table 6 and Table 7.

For the classifying methods, the results of RF are better than that of PNN; all the indexes of RF results are over 96%. For example, the KCs of RF are 99.401 ± 0.121%, 97.491 ± 0.614%, 98.848 ± 0.251%, 98.315 ± 0.445% and 98.652 ± 0.217% for the classifying of elderly subjects vs young subjects, bradycardia subjects vs healthy subjects, tachycardia subjects vs healthy subjects, bradycardia subjects vs tachycardia subjects, and bradycardia subjects vs tachycardia subjects vs healthy subjects, while that of PNN are just 95.953 ± 0.357%, 89.688 ± 1.125%, 91.161 ± 0.699%, 75.572 ± 1.449% and 90.218 ± 0.586%. Particularly for the classification result of bradycardia subjects vs tachycardia subjects using PPN, the KC is only 75.572 ± 1.449% while that of RF is 98.315 ± 0.445%. The KC_2 of PNN is 62.061 ± 1.879%, which means the classifying result for tachycardia subjects is not so good. Meanwhile, the results of TP, FP, FN, and TN indicate that the FP and FN of PNN are obviously higher than that of RF.

For the classifying results between the different groups, it can be inferred from Table 6 that the best performance of RF is the classification between young and elderly subjects. Its KC is 99.401 ± 0.121%, and the values of KC_1 and KC_2 show little difference, which means the performances for the young and the elderly subjects detection are the same. Even for the worst performance of RF, its KC is 97.491 ± 0.614% for the classification of the bradycardia and healthy subjects and is still over 95%, while its KC_2 is 95.880 ± 1.024%,

TABLE 6. The results of classification for different sets.

Classification	Methods	TP	FP	FN	TN	Sp (%)	Se (%)	Ac (%)	KC (%)	KC_2 (%)	KC_1 (%)
O vs Y	PNN	3739±39	57±7	104±12	4100±40	98.626±0.174	97.282±0.300	97.981±0.178	95.953±0.357	94.829±0.564	97.105±0.364
	RF	3832±39	13±4	11±3	4144±39	99.683±0.085	99.720±0.090	99.701±0.060	**99.401±0.121**	99.461±0.173	99.341±0.177
Bc vs Ht	PNN	374±19	19±4	62±8	7546±20	99.747±0.057	85.817±1.731	98.990±0.105	89.688±1.125	85.087±1.798	94.844±1.109
	RF	418±20	3±2	17±4	7561±20	99.956±0.027	96.096±0.973	99.746±0.061	**97.491±0.614**	95.880±1.024	99.163±0.505
Tc vs Ht	PNN	915±25	8±3	146±12	6931±27	99.883±0.044	86.282±1.079	98.079±0.154	91.161±0.699	84.494±1.200	98.983±0.375
	RF	1048±27	9±3	13±3	6931±27	99.877±0.047	98.810±0.324	99.736±0.057	**98.848±0.251**	98.629±0.372	99.069±0.355
Bc vs Tc	PNN	1248±19	12±3	204±12	537±19	97.895±0.593	85.947±0.815	89.221±0.637	75.572±1.449	62.061±1.879	96.659±0.935
	RF	1447±19	9±3	4±2	539±18	98.380±0.479	99.691±0.144	99.331±0.178	**98.315±0.445**	98.865±0.527	97.775±0.659

TABLE 7. The results of classification for healthy, bradycardia and tachycardia subjects.

	Methods	KC_1 (%)	KC_2 (%)	KC_3 (%)	KC (%)
Bc vs Tc vs Ht	PNN	84.680±1.822	83.945±1.165	97.775± 0.439	90.218±0.586
	RF	95.855±0.918	98.805±0.349	99.431±0.220	**98.652±0.217**

so the performance of bradycardia detection needs to be improved. We can also obtain the same conclusion from its Se (96.096 ± 0.973%). For the classification among bradycardia, tachycardia and healthy subjects, the good performance of RF is still maintained. KC is 98.652 ± 0.217%.

IV. DISCUSSION

In this study, the change of pulsatile wave with aging and arrhythmias is quantitatively described by a PSA modeling method we proposed, by which twelve parameters obtained from each pulsatile wave are employed as a feature vector to classify the pulsatile waves from different groups. The two-sample *ks*-test results in Table 4 indicate that there are noticeable differences for all the parameters among different groups. For the 95994 pulsatile waves from Fantasia and 2015 PhysioNet/CinC databases, we extract a 95994×12 feature vector as the data set to train and test classifiers of PNN and RF. From the classifying results in Table 6 and Table 7, the performance of RF is better than that of PNN. For the results of RF, the KCs are over 97% for all classifiers.

However, during training classifiers, we have found the features may be redundant; some features contribute little to the classification results. In addition, the more features we use, the more time we need to spend on training and testing the classifiers. Thus, we explored the relationship between the number of features and the performance of the classifier. For the twelve parameters, we defined 78 combinations of different parameters, and the combination is numbered as *Nu*, $Nu = 1, 2, 3, \ldots$, and 78. As shown in Table 8, combination 1 means the feature vector only contains parameter $\mathbf{A}^1, \ldots$, combination 12 means the feature vector contains all twelve parameters, …, and combination 78 corresponds to the feature vector with the parameter **PPI**. Here, we design the classifiers with RF under these different feature vectors. The samples in training and testing sets still randomly change 100 times when training the classifiers for dropping the influence of the different input samples.

TABLE 8. Different combinations of the model parameters. '-' means null, '*' means the parameter in this row is selected.

P	*Nu*														
	1	2	3	…	11	12	13	14	…	23	24	25	…	33	…	78
$\mathbf{A}^1$	*	*	*	…	*	*	-	-	…	-	-	-	…	-	…	-
$\mathbf{B}^1$	-	*	*	…	*	*	*	*	…	*	-	-	…	-	…	-
$\mathbf{C}^1$	-	-	*	…	*	*	-	*	…	*	*	*	…	*	…	-
$\mathbf{A}^2$	-	-	-	…	*	*	-	-	…	*	-	*	…	*	…	-
$\mathbf{B}^2$	-	-	-	…	*	*	-	-	…	*	-	-	…	*	…	-
$\mathbf{C}^2$	-	-	-	…	*	*	-	-	…	*	-	-	…	*	…	-
$\mathbf{A}^3$	-	-	-	…	*	*	-	-	…	*	-	-	…	*	…	-
$\mathbf{B}^3$	-	-	-	…	*	*	-	-	…	*	-	-	…	*	…	-
$\mathbf{C}^3$	-	-	-	…	*	*	-	-	…	*	-	-	…	*	…	-
K	-	-	-	…	*	*	-	-	…	*	-	-	…	*	…	-
B	-	-	-	…	*	*	-	-	…	*	-	-	…	*	…	-
PPI	-	-	-	…		*	-	-	…	*	-	-	…	*	…	*

Table 9 shows the classifying results between the young and the elderly subjects of the 78 feature vectors. There are 38 feature combinations whose KCs is over 95% (4 - 12, 16 - 23, 27 - 33, 37 - 42, 47 - 50, 56 – 57, and 62 – 63). Among them, the combinations of 4, 16, 27 and 37 all have four features and own the least feature number, their corresponding KCs are 95.626 ± 0.326%, 96.971 ± 0.194%, 95.652 ± 0.274% and 95.847 ± 0.279%. The combination 16 has the best performance and consists of $\mathbf{B}^1$, $\mathbf{C}^1$, $\mathbf{A}^2$, and $\mathbf{B}^2$. Among the combinations consisting of five features (5, 17, 28, 38, 47, and 62), the combination 17 contains $\mathbf{B}^1$, $\mathbf{C}^1$, $\mathbf{A}^2$, $\mathbf{B}^2$, and $\mathbf{C}^2$ and has the best performance with the KC of 98.504 ± 0.134%. Then, with the increase of feature numbers, the performance of classifiers gets better and better. The KCs of combinations 6 - 12 and 18 - 23 are higher than others, while that of 9 to 12 and 20 to 23 show little growth. The combination 20 has the better performance with the KC of 99.473 ± 0.096% and only consists of eight features ($\mathbf{B}^1$, $\mathbf{C}^1$, $\mathbf{A}^2$, $\mathbf{B}^2$, $\mathbf{C}^2$, $\mathbf{A}^3$, $\mathbf{B}^3$, and $\mathbf{C}^3$). The combination 12 with all features has the best performance. KC is 99.543 ± 0.093%.

Moreover, we analyzed the performance of the classifiers for bradycardia, tachycardia and healthy subjects under

TABLE 9. The results of classification for young and old subjects under different feature vectors.

Nu	KC (%)	*Nu*	KC (%)	*Nu*	KC (%)	*Nu*	KC (%)	*Nu*	KC (%)
1	47.769±0.765	**17**	**98.504±0.134**	**33**	**99.054±0.140**	**49**	**97.074±0.273**	65	73.767±0.854
2	80.446±0.788	**18**	**98.830±0.142**	34	42.335±0.719	**50**	**97.284±0.242**	66	79.863±0.649
3	91.133±0.517	**19**	**99.020±0.135**	35	78.463±0.450	51	35.462±0.919	67	90.496±0.437
4	**95.626±0.326**	**20**	**99.473±0.096**	36	91.704±0.505	52	71.058±0.773	68	93.906±0.443
5	**98.454±0.126**	**21**	**99.478±0.121**	**37**	**95.847±0.279**	53	87.118±0.487	69	42.620±0.890
6	**99.085±0.125**	**22**	**99.449±0.134**	**38**	**96.895±0.169**	54	93.528±0.335	70	58.243±1.005
7	**99.335±0.120**	**23**	**99.472±0.112**	**39**	**98.574±0.180**	55	94.446±0.270	71	75.665±0.704
8	**99.430±0.120**	24	11.100±1.077	**40**	**98.633±0.172**	**56**	**95.805±0.306**	72	89.756±0.344
9	**99.519±0.067**	25	63.365±0.819	**41**	**98.773±0.127**	**57**	**96.123±0.238**	73	09.335±1.096
10	**99.522±0.089**	26	89.224±0.411	**42**	**98.837±0.121**	58	38.709±0.986	74	36.134±1.057
11	**99.494±0.084**	**27**	**95.652±0.274**	43	45.779±0.896	59	77.487±0.676	75	67.540±0.917
12	**99.543±0.093**	**28**	**97.493±0.199**	44	73.710±0.660	60	90.625±0.345	76	10.609±1.381
13	33.445±1.135	**29**	**97.818±0.157**	45	88.811±0.388	61	92.610±0.362	77	54.579±0.993
14	77.509±0.645	**30**	**98.940±0.147**	46	93.335±0.389	**62**	**95.047±0.279**	78	28.879±0.729
15	90.269±0.409	**31**	**98.995±0.112**	**47**	**96.527±0.252**	**63**	**95.360±0.307**		
16	**96.971±0.194**	**32**	**98.996±0.147**	**48**	**96.790±0.290**	64	39.237±0.835		

TABLE 10. The results of classification for health, bradycardia, and tachycardia subjects under different feature vectors.

Nu	KC (%)	*Nu*	KC (%)	*Nu*	KC (%)	*Nu*	KC (%)	*Nu*	KC (%)
1	21.702±1.131	17	94.695±0.419	**33**	**98.326±0.260**	**49**	**97.200±0.386**	65	66.896±0.904
2	73.558±0.849	**18**	**96.840±0.301**	34	22.371±1.211	**50**	**97.590±0.369**	66	77.085±0.809
3	83.571±0.697	**19**	**97.780±0.275**	35	66.451±1.135	51	19.478±1.044	67	87.161±0.653
4	90.204±0.554	**20**	**98.188±0.266**	36	83.410±0.632	52	69.364±1.088	68	93.300±0.556
5	94.935±0.379	**21**	**98.107±0.312**	37	94.507±0.492	53	90.240±0.471	69	20.218±0.878
6	**96.318±0.400**	**22**	**98.092±0.272**	**38**	**96.845±0.356**	**54**	**95.667±0.539**	70	51.110±1.283
7	**97.788±0.208**	**23**	**98.315±0.305**	**39**	**97.765±0.362**	**55**	**96.024±0.392**	71	72.771±1.003
8	**98.096±0.246**	24	18.394±1.197	**40**	**97.686±0.376**	**56**	**96.297±0.351**	72	90.976±0.608
9	**98.429±0.272**	25	58.631±1.174	**41**	**97.646±0.301**	**57**	**96.911±0.404**	73	23.997±1.313
10	**98.430±0.284**	26	84.465±0.764	**42**	**98.000±0.353**	58	22.297±1.205	74	52.554±1.228
11	**98.371±0.267**	27	92.966±0.430	43	30.471±0.924	59	67.070±1.278	75	82.754±0.747
12	**98.602±0.228**	**28**	**96.267±0.418**	44	62.816±0.933	60	86.332±0.750	76	18.051±1.023
13	23.728±0.858	**29**	**97.515±0.360**	45	89.872±0.532	61	89.540±0.564	77	80.656±0.815
14	46.654±0.922	**30**	**98.160±0.319**	**46**	**95.135±0.430**	62	92.059±0.572	78	73.304±0.753
15	77.991±0.750	**31**	**98.095±0.289**	**47**	**97.144±0.400**	63	94.665±0.436		
16	90.524±0.571	**32**	**98.111±0.327**	**48**	**97.195±0.406**	64	26.149±1.143		

78 feature vectors. The results are shown in Table 10. There are 33 feature combinations with the KCs over 95%, which are shown in bold in Table 10. Among these feature combinations, 46 and 54 only have four features while their KCs are 95.135 ± 0.430% and 95.667 ± 0.539%, respectively. The combination 54 has the features of $\mathbf{C}^2$, $\mathbf{A}^3$, $\mathbf{B}^3$ and $\mathbf{C}^3$. Similar to the results of the classifying between the young and elderly subjects, the performances of the classifiers are still getting better and better with the increasing of feature numbers. The KCs of combinations 9 - 12 are higher than others but show little growth. The combination 9 has a good performance with the KC of 98.429 ± 0.272% and consists of $\mathbf{A}^2, \mathbf{B}^1, \mathbf{C}^1, \mathbf{A}^2, \mathbf{B}^2, \mathbf{C}^2, \mathbf{A}^3, \mathbf{B}^3$, and $\mathbf{C}^3$. The best performance still is combination 12 who owns all the features.

The aim of the 2015 physioNet/CinC Challenge was to develop the methods to reduce the incidence of false alarms in intensive care unit. These false alarms are attributed to the abnormal segments generated from the movement artifact, sensor disconnects, and other events. So far, many algorithms are proposed to distinguish between these abnormal segments and pathological signal segments and to detect the episodes of these life-threatening arrhythmias. In [59] authors trained classification model with SVM to detect the five kinds of arrhythmias. The results of the training set for EB were Se = 100% and Sp = 93%, and that of for ET were Se = 100% and Sp = 89%. Bonomi *et al.* [60] extracted PR from PPG signal to detect the episodes of bradycardia (Se = 85.0%, Sp = 99.4%) and tachycardia (Se = 89.1%, Sp = 99.9%). Zong *et al.* [61] proposed using PBIs, pulse waveform amplitude and maximum slope, pulse signal quality, and the pulse rhythm to reduce false alarms. The results show that the algorithm retains all (100%) of the true alarms and markedly reduces the false alarms. Lameski *et al.* [62] performed an automated feature engineering and machine learning algorithms to suppress the false alarms using ABP signals. The best results of EB are Se = 83.60% and Sp = 98.77%, that of ET are 99.43% and 89.86%. These methods are efficient in detecting the episodes of the life-threaten arrhythmias, and most of them just rely on PR can achieve their purpose. As shown in Fig.6, the green line is the standard of the PR to detect EB and ET. The segments of $Bc(1)$, $Bc(2)$ and $Tc(1)$ are the processes of arrhythmia outbursts, the PR in this duration is rapidly changed and then recovered to the normal range, thus, it is easy to capture the episodes of these

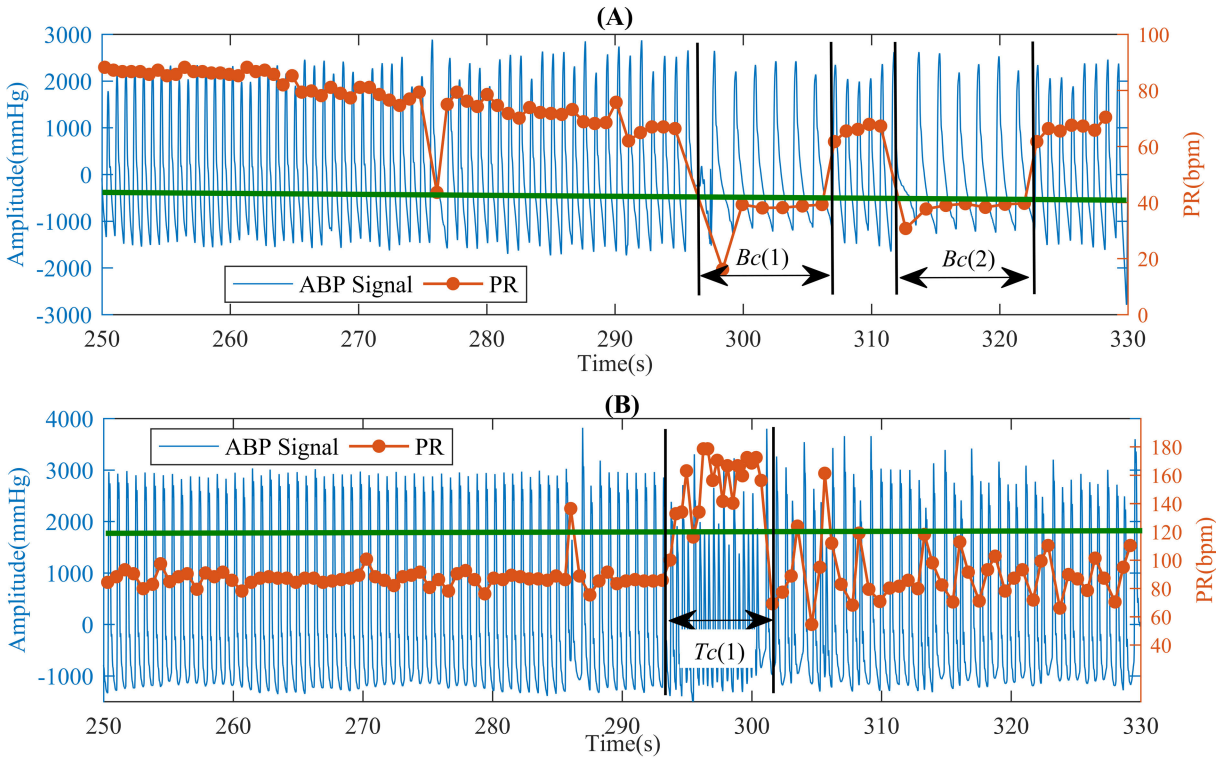

FIGURE 6. Two ABP signals and their pulsatile rates for one subject with extreme bradycardia (A) and one with extreme tachycardia (B).

TABLE 11. The classification performance of the proposed method and comparison with former studies.

Methods	KC (%)			
	Bc vs Ht	Tc vs Ht	Bc vs Tc	Bc vs Tc vs Ht
McManus et al. [63]	72.265±1.499	87.797±1.086	76.847±0.849	81.442±0.112
Lee et al. [27]	55.778±0.385	72.155±1.777	68.097±0.338	67.016±0.281
Fallet et al. [29]	54.870±4.297	71.034±0.164	66.391±0.704	67.046±0.248
Eerikäinen et al. [58]	86.936±3.850	98.830±0.137	93.935±0.280	94.863±0.505
This work	97.855±0.489	99.022±0.228	98.698±0.362	98.652±0.217

two arrhythmias by PR. However, it is more important to confirm bradycardia and tachycardia before they deteriorate into the life-threatening malignant arrhythmias. According to their definitions in introduction, we detected them by the PR. Results are shown in Table 10, where the KC of combination 78 corresponding to the feature of PR is just $73.304 \pm 0.753\%$. Fig. 6 illustrates the reasons the PRs in un-outburst segments are within the normal range. Thus, we need to derive more information from pulsatile signal to improve the detection results.

Recently, some studies have tried to extract information from PBIs and its derivatives for detecting some arrhythmias, e.g. AF, premature atrial contraction, and premature ventricular contraction. Although they are not engaged to directly detect bradycardia and tachycardia, we try their method in our works. We chose four methods to classify the pulsatile waves from our experimental dataset. Here, the classifiers are trained by RF. The results are in Table 11. The performance of our proposed method is the best, where the KCs of different classifiers are higher than that of other methods. In [63], the features they used are RMSSD, turning point ratio (TPR) and ShE from PBIs. The features in [27] are RMSSD and ShE. In [29], the PBIs features are mean, standard deviation, interquartile range, minimum, maximum and RMSSD. The ShE, RMSSD, normalized RMSSD, PNN40, PNN70, sample entropy (SampE) and coefficient of sample entropy (CosEn) of PBIs are used in [58]. The features they used are all from PBIs of pulsatile waves, while the features we extracted are the PBIs and the parameters of PSA models which are used to describe the change of waveform. The PBIs and its derivatives can reflect the change of heartbeat rhythm, and some parameters of PSA contain the information about hemodynamics. Therefore, our proposed method has better performance.

We can infer from the experimental results that the PSA modeling method is effective in quantitative describing the changes of pulsatile wave, and we can obtain some valuable physiological and pathological information from the models of the different subjects. All the model parameters

are markedly different among the different groups and are useful for bradycardia and tachycardia detection with high performance even if we do not do cross-validation in training classifiers. However, we found some of the features may be redundant in detecting bradycardia and tachycardia. Although we obtained some efficient feature combinations, they vary with the different classification and are limited in generalization. Thus, future works are needed in selecting the optimal PSA model or using a more cost-effective classification method (e.g., deep learning) in bradycardia and tachycardia detection. In addition, there are three other arrhythmias (asystole, ventricular tachycardia, and ventricular flutter/fibrillation) in the database of the 2015 PhysioNet/CinC Challenge. We will improve our proposed method to detect these arrhythmias in the future.

V. CONCLUSION

In this study, a bradycardia and tachycardia detection method with PSA modeling is presented. We used the PSA modeling method to quantitatively describe the change of pulsatile waves, and twelve parameters about the heartbeat rhythm and homodynamic were extracted from the model of each pulsatile wave. The proposed method was employed to analyze the ABP signals of the healthy subjects from the Fantasia database and of the bradycardia and tachycardia subjects from the 2015 PhysioNet/CinC Challenge database. We obtain the models of the young, elderly, healthy, bradycardia and tachycardia subjects and extract some physiological and pathological information from these models. Then, the models' parameters were engaged to train the classifiers with PNN and RF. The results show that the performance of classifiers based on RF is better than that based on PNN. The KCs of all classifier are over 97% which is better than the performance of the former studies. It suggests that the proposed method is efficient to detect bradycardia and tachycardia and has the potential to diagnose these two arrhythmias in m-health. In the future, we will continue to improve the proposed method and try to use it to diagnose other cardiac arrhythmias.

REFERENCES

[1] Q. Zhang, X. Chen, Z. Fang, Q. Zhan, T. Yang, and S. Xia, "Reducing false arrhythmia alarm rates using robust heart rate estimation and cost-sensitive support vector machines," *Physiol. Meas.*, vol. 38, no. 2, pp. 259–271, Jan. 2017.

[2] Y. Xia and Y. Xie, "A novel wearable electrocardiogram classification system using convolutional neural networks and active learning," *IEEE Access*, vol. 7, pp. 7989–8001, 2019.

[3] Y. Xia, H. Zhang, L. Xu, Z. Gao, H. Zhang, H. Liu, and S. Li, "An automatic cardiac arrhythmia classification system with wearable electrocardiogram," *IEEE Access*, vol. 6, pp. 16529–16538, 2018.

[4] H. Li, X. Wang, L. Chen, and E. Li, "Denoising and R-peak detection of electrocardiogram signal based on EMD and improved approximate envelope," *Circuits, Syst., Signal Process.*, vol. 33, no. 4, pp. 1261–1276, 2014.

[5] M. S. Cetin, E. H. O. Cetin, U. Canpolat, S. Cay, S. Topaloglu, A. Temizhan, and S. Aydogdu, "Usefulness of fragmented QRS complex to predict arrhythmic events and cardiovascular mortality in patients with noncompaction cardiomyopathy," *Amer. J. Cardiol.*, vol. 117, no. 9, pp. 1516–1523, May 2016.

[6] H. Li and X. Wang, "Detection of electrocardiogram characteristic points using lifting wavelet transform and Hilbert transform," *Trans. Inst. Meas. Control*, vol. 35, no. 5, pp. 574–582, 2013.

[7] H. J. Trappe, "ECG results: Tips and tricks for the correct diagnosis: Bradycardia and tachycardia rhythm disorders," *Herz*, vol. 43, no. 2, pp. 177–194, Mar. 2018.

[8] H. Li, X. Feng, L. Cao, E. Li, H. Liang, and X. Chen, "A new ECG signal classification based on WPD and ApEn feature extraction," *Circuits, Syst., Signal Process.*, vol. 35, no. 1, pp. 339–352, Jan. 2016.

[9] C. Ye, B. V. K. V. Kumar, and M. T. Coimbra, "An automatic subject-adaptable heartbeat classifier based on multiview," *IEEE J. Biomed. Health. Inf.*, vol. 20, no. 6, pp. 1485–1492, Nov. 2016.

[10] Z. Mei, X. Gu, H. Chen, and W. Chen, "Automatic atrial fibrillation detection based on heart rate variability and spectral features," *IEEE Access*, vol. 6, pp. 53566–53575, 2018.

[11] B. N. Schaeffer, M. Rybczynski, S. Sheikhzadeh, R. Ö. Akbulak, J. Moser, M. Jularic, D. Schreiber, A. Daubmann, S. Willems, Y. von Kodolitsch, and B. A. Hoffmann, "Heart rate turbulence and deceleration capacity for risk prediction of serious arrhythmic events in Marfan syndrome," *Clin. Res. Cardiol.*, vol. 104, no. 12, pp. 1054–1063, Dec. 2015.

[12] S. S. Al-Zaiti, G. Pietrasik, M. G. Carey, M. Alhamaydeh, J. M. Canty, and J. A. Fallavollita, "The role of heart rate variability, heart rate turbulence, and deceleration capacity in predicting cause-specific mortality in chronic heart failure," *J. Electrocardiol.*, vol. 52, pp. 70–74, Jan./Feb. 2019.

[13] M. Hammad, A. Maher, K. Wang, F. Jiang, and M. Amrani, "Detection of abnormal heart conditions based on characteristics of ECG signals," *Measurement*, vol. 125, pp. 634–644, Sep. 2018.

[14] M. Amrani, M. Hammad, F. Jiang, K. Wang, and A. Amrani, "Very deep feature extraction and fusion for arrhythmias detection," *Neural Comput. Appl.*, vol. 30, no. 7, pp. 2047–2057, Oct. 2018.

[15] M. Hammad, Y. Liu, and K. Wang, "Multimodal biometric authentication systems using convolution neural network based on different level fusion of ECG and fingerprint," *IEEE Access*, vol. 7, pp. 26527–26542, 2019.

[16] H. Li, D. Yuan, X. Ma, D. Cui, and L. Cao, "Genetic algorithm for the optimization of features and neural networks in ECG signals classification," *Sci. Rep.*, vol. 7, p. 41011, Jan. 2017.

[17] H. Li, H. Liang, C. Miao, L. Cao, X. Feng, C. Tang, and E. Li, "Novel ECG signal classification based on KICA nonlinear feature extraction," *Circuits, Syst. Signal Process.*, vol. 35, no. 4, pp. 1187–1197, Apr. 2015.

[18] P. Mohapatra, P. S. Premkumar, and M. Sivaprakasam, "A yellow–orange wavelength-based short-term heart rate variability measurement scheme for wrist-based wearables," *IEEE Trans. Instrum. Meas.*, vol. 67, no. 5, pp. 1091–1101, May 2018.

[19] P. M. Middleton, G. S. H. Chan, E. Steel, P. Malouf, C. Critoph, G. Flynn, E. O'Lone, B. G. Celler, and N. H. Lovell, "Fingertip photoplethysmographic waveform variability and systemic vascular resistance in intensive care unit patients," *Med. Biol. Eng. Comput.*, vol. 49, no. 8, pp. 859–866, Aug. 2011.

[20] P. M. Middleton, G. S. H. Chan, S. Marr, B. G. Celler, and N. H. Lovell, "Identification of high-risk acute coronary syndromes by spectral analysis of ear photoplethysmographic waveform variability," *Physiol. Meas.*, vol. 32, no. 8, pp. 1181–1192, Jun. 2011.

[21] Y. Sun and N. Thakor, "Photoplethysmography revisited: From contact to noncontact, from point to imaging," *IEEE Trans. Biomed. Eng.*, vol. 63, no. 3, pp. 463–477, Mar. 2016.

[22] Y. Chou, P. Zhu, X. Huang, J. Lin, J. Liu, and Y. Gu, "Comparison between heart rate variability and pulse rate variability for bradycardia and tachycardia subjects," in *Proc. ICCAIS*, Hangzhou, China, Oct. 2018, pp. 1–6.

[23] K. Lan, P. Raknim, W.-F. Kao, and J.-H. Huang, "Toward hypertension prediction based on PPG-derived HRV signals: A feasibility study," *J. Med. Syst.*, vol. 42, p. 103, Jun. 2018.

[24] Y. Chen and W. Chen, "Long-term tracking of a patient's health condition based on pulse rate dynamics during sleep," *Ann. Biomed. Eng.*, vol. 39, pp. 2922–2934, Dec. 2011.

[25] A. Hochstadt, E. Chorin, S. Viskin, A. L. Schwartz, N. Lubman, and R. Rosso, "Continuous heart rate monitoring for automatic detection of atrial fibrillation with novel bio-sensing technology," *J. Electrocardiol.*, vol. 52, pp. 23–27, Jan. 2019.

[26] E. Gil, P. Laguna, J. Martínez, O. Barquero-Pérez, A. García-Alberola, and L. Sornmo, "Heart rate turbulence analysis based on photoplethysmography," *IEEE Trans. Biomed. Eng.*, vol. 60, no. 11, pp. 3149–3155, Nov. 2013.

[27] K. Lee, H. O. Choi, S. D. Min, J. Lee, B. B. Gupta, and Y. Nam, "A comparative evaluation of atrial fibrillation detection methods in Koreans based on optical recordings using a smartphone," *IEEE Access*, vol. 5, pp. 11437–11443, 2017.
[28] J. W. Chong, N. Esa, D. D. McManus, and K. H. Chon, "Arrhythmia discrimination using a smart phone," *IEEE J. Biomed. Health. Inf.*, vol. 19, no. 3, pp. 815–824, May 2015.
[29] S. Fallet, M. Lemay, P. Renevey, C. Leupi, E. Pruvot, and J.-M. Vesin, "Can one detect atrial fibrillation using a wrist-type photoplethysmographic device," *Med. Biol. Eng. Comput.*, vol. 57, no. 2, pp. 477–487, Feb. 2019.
[30] R. Couceiro, P. Carvalho, R. P. Paiva, J. Henriques, I. Quintal, M. Antunes, J. Muehlsteff, C. Eickholt, C. Brinkmeyer, M. Kelm, and C. Meyer, "Assessment of cardiovascular function from multi-Gaussian fitting of a finger photoplethysmogram," *Physiol. Meas.*, vol. 36, no. 9, pp. 1801–1825, Aug. 2015.
[31] D. Martin-Martinez, P. Casaseca-de-la-Higuera, M. Martin-Fernandez, and C. Alberola-Lopez, "Stochastic modeling of the PPG signal: A synthesis-by-analysis approach with applications," *IEEE Trans. Biomed. Eng.*, vol. 60, no. 9, pp. 2432–2441, Sep. 2013.
[32] T. Tigges, A. Pielmus, M. Klum, A. Feldheiser, O. Hunsicker, and R. Orglmeister, "Model selection for the pulse decomposition analysis of fingertip photoplethysmograms," in *Proc. 39th Annu. Int. Conf. IEEE Eng. Med. Biol. Soc. (EMBC)*, Jul. 2017, pp. 4014–4017.
[33] X. Jiang, S. Wei, J. Ji, F. Liu, P. Li, and C. Liu, "Modeling radial artery pressure waveforms using curve fitting: Comparison of four types of fitting functions," *Artery Res.*, vol. 23, pp. 56–62, Sep. 2018.
[34] Y. X. Chou, A. H. Zhang, and P. Wang, "Pulse rate variability estimation method based on sliding window iterative DFT and Hilbert transform," *J. Med. Biol. Eng.*, vol. 34, no. 4, pp. 347–355, Aug. 2014.
[35] A. M. Alqudah, "An enhanced method for real-time modelling of cardiac related biosignals using Gaussian mixtures," *J. Med. Eng. Technol.*, vol. 41, no. 8, pp. 600–611, 2017.
[36] A. Sološenko, A. Petrėnas, V. Marozas, and L. Sörnmo, "Modeling of the photoplethysmogram during atrial fibrillation," *Comput. Biol. Med.*, vol. 81, pp. 130–138, Feb. 2017.
[37] S. C. Huang, H. Y. Jan, and W. C. Lin, "Evaluation of decomposition analysis on multi-models for digital volume pulse signal," in *World Congress on Medical Physics and Biomedical Engineering*. Toronto, ON, Canada: Springer, 2015, pp. 1731–1734.
[38] D. He, L. Wang, X. Fan, Y. Yao, N. Geng, Y. Sun, and W. Qian, "A new mathematical model of wrist pulse waveforms characterizes patients with cardiovascular disease—A pilot study," *Med. Eng. Phys.*, vol. 48, pp. 142–149, Oct. 2017.
[39] L. Wang, L. Xu, D. Zhao, Y. Yao, and D. Song, "FPGA-based design and implementation of arterial pulse wave generator using piecewise Gaussian-cosine fitting," *Comput. Biol. Med.*, vol. 59, pp. 142–151, Apr. 2015.
[40] C. Liu, D. Zheng, A. Murray, and C. Liu, "Modeling carotid and radial artery pulse pressure waveforms by curve fitting with Gaussian functions," *Biomed. Signal Process. Control*, vol. 8, no. 5, pp. 449–454, Sep. 2013.
[41] N. Paradkar and S. R. Chowdhury, "Cardiac arrhythmia detection using photoplethysmography," in *Proc. 39th Annu. Int. Conf. IEEE Eng. Med. Biol. Soc. (EMBC)*, South Korea, Jul. 2017, pp. 113–116.
[42] B. Sun, C. Wang, X. Chen, Y. Zhang, and H. Shao, "PPG signal motion artifacts correction algorithm based on feature estimation," *Optik*, vol. 176, pp. 337–349, Jan. 2018.
[43] M. Sorelli, A. Perrella, and L. Bocchi, "Detecting vascular age using the analysis of peripheral pulse," *IEEE Trans. Biomed. Eng.*, vol. 65, no. 12, pp. 2742–2750, Dec. 2018.
[44] N. Paradkar and S. R. Chowdhury, "Coronary artery disease detection using photoplethysmography," in *Proc. 39th Annu. Int. Conf. IEEE Eng. Med. Biol. Soc. (EMBC)*, South Korea, Jul. 2017, pp. 100–103.
[45] X. He, R. A. Goubran, and X. P. Liu, "Secondary peak detection of PPG signal for continuous cuffless arterial blood pressure measurement," *IEEE Trans. Instrum. Meas.*, vol. 63, no. 6, pp. 1431–1439, Jun. 2014.
[46] C. Liu, D. Zheng, L. Zhao, and C. Liu, "Gaussian fitting for carotid and radial artery pressure waveforms: Comparison between normal subjects and heart failure patients," *Biomed. Mater. Eng.*, vol. 24, no. 1, pp. 271–277, Jan. 2014.
[47] A. L. Goldberger, L. A. Amaral, L. Glass, J. M. Hausdorff, P. C. Ivanov, R. G. Mark, J. E. Mietus, G. B. Moody, C. K. Peng, and H. E. Stanley, "Physiobank, physiotoolkit, and physionet: Components of a new research resource for complex physiologic signals," *Circulation*, vol. 101, no. 23, pp. e215–e220, Jun. 2000.
[48] G. D. Clifford, I. Silva, B. Moody, Q. Li, D. Kella, A. Shahin, T. Kooistra, D. Perry, and R. G. Mark, "The physionet/computing in cardiology challenge 2015: Reducing false arrhythmia alarms in the ICU," in *Proc. CinC*, Nice, France, Sep. 2015, pp. 273–276.
[49] Y. X. Chou, A. H. Zhang, and B. Yang, "Age-related alterations in the sign series entropy of short-term pulse rate variability," *Neurocomputing*, vol. 228, pp. 213–219, Mar. 2017.
[50] A. Hernando, M. D. Peláez-Coca, M. T. Lozano, M. Aiger, D. Izquierdo, A. Sánchez, M. I. López-Jurado, I. Moura, J. Fidalgo, J. Lázaro, and E. Gil, "Autonomic nervous system measurement in hyperbaric environments using ECG and PPG signals," *IEEE J. Biomed. Health. Inf.*, vol. 23, no. 1, pp. 132–142, Jan. 2019.
[51] A. Solosenko, A. Petrenas, and V. Marozas, "Photoplethysmography-based method for automatic detection of premature ventricular contractions," *IEEE Trans. Biomed. Circuits Syst.*, vol. 9, no. 5, pp. 662–669, Oct. 2015.
[52] T. Tigges, J. Rockstroh, A. Pielmu, M. Klum, A. Feldheiser, O. Hunsicker, and R. Orglmeister, "In-ear photoplethysmography for central pulse waveform analysis in non-invasive hemodynamic monitoring," *Current Directions Biomed. Eng.*, vol. 3, no. 2, pp. 587–590, 2017.
[53] M. Nosrati and N. Tavassolian, "High-accuracy heart rate variability monitoring using Doppler radar based on Gaussian pulse train modeling and FTPR algorithm," *IEEE Trans. Microw. Theory Techn.*, vol. 66, no. 1, pp. 556–567, Jan. 2018.
[54] Y. Chou, B. Xu, Y. Gu, R. Zhang, L. Wang, and Y. Jin, "A fast mathematical morphology filter on one dimensional sampled signal," in *Proc. ICCAIS*, Chiang Mai, Thailand, Oct. 2017, pp. 233–238.
[55] Y. Teng, L. Ge, and Y. X. Chou, "A novel abnormal segments detection method for photopletysmography signal," in *Proc. CCC*, Wuhan, China, Jul. 2018, pp. 4113–4117.
[56] A. Liaw and M. Wiener, "Classification and regression by randomforest," *R News*, vol. 2, no. 3, pp. 18–22, 2002.
[57] M. S. Islam, W. Khreich, and A. Hamou-Lhadj, "Anomaly detection techniques based on kappa-pruned ensembles," *IEEE Trans. Rel.*, vol. 67, no. 1, pp. 212–229, Mar. 2018.
[58] L. M. Eerikäinen, A. G. Bonomi, F. Schipper, L. R. C. Dekker, R. Vullings, H. M. de Morree, and R. M. Aarts, "Comparison between electrocardiogram- and photoplethysmogram-derived features for atrial fibrillation detection in free-living conditions," *Physiol. Meas.*, vol. 39, no. 8, Aug. 2018, Art. no. 084001.
[59] V. Kalidas and L. S. Tamil, "Cardiac arrhythmia classification using multi-modal signal analysis," *Physiolog. Meas.*, vol. 37, no. 8, pp. 1253–1272, Jul. 2016.
[60] A. G. Bonomi, L. M. Eerikäinen, F. Schipper, R. M. Aarts, H. M. de Morree, and L. Dekker, "Detecting episodes of brady- and tachycardia using photo-plethysmography at the wrist in free-living conditions," in *Proc. CinC*, Rennes, France, Sep. 2017, pp. 1–4.
[61] W. Zong, L. Nielsen, B. Gross, J. Brea, and J. Frassica, "A practical algorithm to reduce false critical ECG alarms using arterial blood pressure and/or photoplethysmogram waveforms," *Physiolog. Meas.*, vol. 37, no. 8, pp. 1355–1369, Jul. 2016.
[62] P. Lameski, E. Zdravevski, S. Koceski, A. Kulakov, and V. Trajkovik, "Suppression of intensive care unit false alarms based on the arterial blood pressure signal," *IEEE Access*, vol. 5, pp. 5829–5836, 2017.
[63] D. D. McManus, J. W. Chong, A. Soni, J. S. Saczynski, N. Esa, C. Napolitano, C. E. Darling, E. Boyer, R. K. Rosen, K. C. Floyd, and K. H. Chon, "PULSE-SMART: Pulse-based arrhythmia discrimination using a novel smartphone application," *J. Cardiovasc. Electrophysiol.*, vol. 27, no. 1, pp. 51–57, 2016.

YONGXIN CHOU was born in Wangzhuang, Qingyang, Gansu, China, in 1987. He received the B.S. and Ph.D. degrees from the College of Electrical and Information Engineering, Lanzhou University of Technology, Lanzhou, China, in 2010 and 2015, respectively. In January 2016, he joined the School of Electrical and Automatic Engineering, Changshu Institute of Technology, Suzhou, China, where he is currently a Lecturer. He is also a Postdoctoral Researcher with the East China University of Science and Technology, Research Institute of Changshu Company Ltd. His main research interests include physiological signal measurement and analysis, cardiovascular disease detection, and machine learning.

JASON GU is currently a Professor of robotics and assistive technology with the Department of Electrical and Computer Engineering, Dalhousie University. He has published more than 300 journals, book chapters and conference articles. His research interests include biomedical engineering, biosignal processing, rehabilitation engineering, neural networks, robotics, mechatronics, and control. He is the IEEE member of SMC and RAS. He is also a Fellow of the Engineering Institute of Canada and the Canada Academy of Engineering. He has been an Editor of the *Journal of Control and Intelligent Systems*, the *Transactions on CSME*, the IEEE TRANSACTIONS ON MECHATRONICS, the *IEEE SMC Magazine*, the *International Journal of Robotics and Automation*, and IEEE ACCESS. He is also the IEEE Canada President-Elect, from 2018 to 2019.

JICHENG LIU received the B.S. degree from the School of Electrical and Information Engineering, Northeast Petroleum University, Daqing, China, in 1997, and the Ph.D. degree from the College of Electronics and Information, Beihang University, Beijing, China, in 2003. From 2007 to 2016, he was a Professor with Northeast Petroleum University. In 2017, he joined the School of Electric and Automation Engineering, Changshu Institute of Technology, Suzhou, China. His research interests include non-stationary signal analysis and seismic processing.

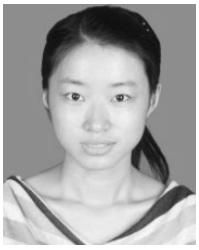

YA GU was born in Taizhou, China. She received the B.Sc. degree from the Yancheng Institute of Technology, in 2010, and the M.Sc. and Ph.D. degrees in automatic control from Jiangnan University, Wuxi, China, in 2012 and 2015, respectively. She was a visiting Ph.D. student with the University of Alberta, Edmonton, AB, Canada, from 2014 to 2015. She is currently a Senior Lecturer with the School of Electrical and Automatic Engineering, Changshu Institute of Technology, Suzhou, China. Her current research interests include model identification and adaptive control.

JIAJUN LIN received the Ph.D. degree from Tsinghua University, Beijing, China, in 1998. He is currently a Professor with the School of Information Science and Engineering, East China University of Science and Technology, Shanghai, China. His research interests include signal processing and information security. He is a member of the Intelligent Control Professional Committee of China Automation Society and the Automation Committee of Shanghai Automation Society.